

## Chaotic Frequency Scaling in a Coupled Oscillator Model for Free Rhythmic Actions

**Aaron Raftery**

*araftery@psu.edu*

*Department of Kinesiology, Pennsylvania State University,  
University Park, PA 16802, U.S.A.*

**Joseph Cusumano**

*jpc3@psu.edu*

*Department of Engineering Science and Mechanics, Pennsylvania State University,  
University Park, PA 16802, U.S.A.*

**Dagmar Sternad**

*dxs48@psu.edu*

*Department of Kinesiology, Pennsylvania State University,  
University Park, PA 16802, U.S.A.*

The question of how best to model rhythmic movements at self-selected amplitude-frequency combinations, and their variability, is a long-standing issue. This study presents a systematic analysis of a coupled oscillator system that has successfully accounted for the experimental result that humans' preferred oscillation frequencies closely correspond to the linear resonance frequencies of the biomechanical limb systems, a phenomenon known as resonance tuning or frequency scaling. The dynamics of the coupled oscillator model is explored by numerical integration in different areas of its parameter space, where a period doubling route to chaotic dynamics is discovered. It is shown that even in the regions of the parameter space with chaotic solutions, the model still *effectively* scales to the biomechanical oscillator's natural frequency. Hence, there is a solution providing for frequency scaling in the presence of chaotic variability. The implications of these results for interpreting variability as fundamentally stochastic or chaotic are discussed.

### 1 Introduction ---

Rhythmic behaviors performed at self-selected amplitude-frequency combinations are ubiquitous in the animal kingdom. From leg swinging in walking humans to tail beating in swimming fish to wing flapping in avian flight, rhythmic actions provide the fundamental means for animals to move about and interact with their environments. Researchers have long recognized the

phylogenetic significance of this class of movements and have sought to discover organizing principles from their experimental characterizations. Following Scripture's early inquiries (1899), rhythmic behaviors performed at self-selected frequencies and amplitudes will be referred to as *free rhythmic actions*. The alternative form of rhythmic behaviors, which Scripture named *regulated rhythmic actions*, involves the adoption of an externally determined movement pace, independent of the animal's preferred rhythmic motions. The focus of this letter is on free rhythmic actions and their principles of organization.

Confronted with the complexity of the different neuromuscular systems that produce these coordinated rhythmic movements, many investigators of locomotory actions and intermanual coordination have employed simplified mathematical models to guide their respective experimental research. One class of models that has provided an entry into the subject comprises linear oscillators of the form

$$\ddot{x} + \zeta \dot{x} + \lambda^2 x = f(t), \quad (1.1)$$

where  $x$  is position,  $\zeta$  is the linear damping coefficient,  $\lambda$  is the biomechanical system's natural frequency in the absence of damping, and  $f(t)$  is a periodic forcing function that represents signals from the animal's neuromuscular system to drive the biomechanical oscillatory system (Demont, 1988; Demont & Gosline, 1988; Greenewalt, 1960). One benefit of using models of the form of equation 1.1 is that their linearity allows a full characterization of the model's behavior from frequency response functions. By estimating the parameters  $\zeta$  and  $\lambda$  and comparing the calculated resonance frequencies to experimentally observed oscillation frequencies in intact animals, researchers have been able to show considerable support for the hypothesis that the self-selected frequencies in free rhythmic actions of a variety of animals closely correspond to the linear resonance frequencies of the oscillating limb systems.

This result is intuitively appealing because operating at resonance leads to a maximal oscillation amplitude for minimal forcing input from the neuromuscular system, thereby minimizing the animal's energy expenditure. Examples that show the diversity of the biomechanical systems that have been modeled as linear oscillators to support this hypothesis are the wings of insects and birds (Greenewalt, 1960), the shells of scallops (Demont, 1988), the bells of jellyfish (Demont & Gosline, 1988), and humans, as discussed below. In this letter, we refer to the phenomenon of an animal scaling its self-selected frequency to the relevant biomechanical natural frequency as *resonance tuning* or *frequency scaling*.

While linear models of the form of equation 1.1 are useful in guiding the experiments cited above, further experimental work has also shown their limitations. One example is the limited range of behaviors that the model is

capable of producing. The linearity of equation 1.1 implies that the only way for the system to produce irregular or variable behavior is through irregular forcing input. This means that any attempt to reconcile equation 1.1 with the variability inherent in free rhythmic action must include variability in the external forcing (see Riley & Turvey, 2002, for a review on variability in human movements). The reliance on external forcing has not compromised the experimental work cited above, because it focused primarily on estimating the parameters of the left side of equation 1.1 in order to investigate the existence of frequency scaling. However, the nonautonomous form of equation 1.1 does not facilitate the study of how the rhythmic motions with their associated frequency scalings are internally generated by the organism. Further, no insight about the origin of variability could be gained.

A number of studies of frequency scaling in free rhythmic actions of humans have already addressed the problem of nonautonomy in their models and replaced the external forcing term in equation 1.1 with a function  $F(x, \dot{x})$ , dependent on only the current state of the biomechanical system (Beek & Beek, 1988; Goldfield, Kay, & Warren, 1993; Holt, Hamill, & Andres, 1990; Kugler & Turvey, 1987; Kay, Kelso, Saltzman, & Schönner, 1987), thus removing any explicit time dependence in the system:

$$\ddot{x} + \zeta \dot{x} + \lambda^2 x = F(x, \dot{x}). \quad (1.2)$$

Autonomous models are able to account for the properties of free rhythmic actions without taking out a "loan of intelligence" by unexplained external forcing terms (Dennett, 1971; Kugler & Turvey, 1987). Experimental results complementing such modeling again indicated frequency scaling behavior in hand-held pendulum swinging (Kugler & Turvey, 1987; Yu, Russell, & Sternad, 2003), walking (Holt et al., 1990; Holt, Saltzman, Ho, Kubo, & Ulrich, 2006), and infant bouncing in spring-harness systems (Goldfield et al., 1993). Although invoking models of the form of equation 1.2 does solve the problem of reliance on external forcing, the implicit two-dimensional phase space limits the steady-state dynamics to periodic and fixed-point behaviors. This means that, similar to equation 1.1, the only option for modeling the spatiotemporal variability of free rhythmic actions using the form of equation 1.2 is again to include external sources of this variability. In addition, models of this type still do not provide any insight into how the neuromuscular system works since they separate the mechanical from the neurophysiological levels of description. Specifically, equation 1.2 does not possess any neurological state variable.

Another class of models that has been developed for free rhythmic actions that aims to overcome the limitations of those relying on external forcing terms is based on coupled autonomous oscillators (Hatsopoulos, 1996; Williamson, 1998; Wenderoth & Bock, 1999; Sternad, Saltzman, &

Turvey, 1998). Such models consist of some form of internal oscillator representing a central pattern generator (CPG) with bidirectional coupling to a linear oscillator representing the biomechanical limb. The advantages of such a model structure in accounting for rhythmic movements have been discussed by Beek, Peper, and Daffertshofer (2002). The model explored in this letter is an example of such a system and was initially proposed by Hatsopoulos (1996).

Hatsopoulos introduced a van der Pol oscillator to represent the CPG in order to drive the biomechanical oscillator of equation 1.1, representing a pure torque driver acting on a linearized pendulum. The coupled system included feedback from the biomechanical oscillator to the CPG frequency to allow resonance tuning or frequency scaling at the biomechanical level:

$$\ddot{y} + \varepsilon(y^2 - 1)\dot{y} + (\omega + Bx)^2y = 0 \quad (1.3a)$$

$$\ddot{x} + \lambda^2x = Gy \quad (1.3b)$$

where  $y$  is the output of the CPG,  $x$  is the output of the biomechanical oscillator,  $\varepsilon$  is a parameter that determines the strength of the nonlinearity in the CPG's oscillations,  $\omega$  is the CPG's frequency in the absence of sensory feedback,  $B$  is an "afferent" gain constant for  $x$ , and  $G$  is an "efferent" gain constant for  $y$ . Damping in the biomechanical oscillator, equation 1.3b has been assumed negligible ( $\zeta = 0$ ). Importantly, the nonlinearity in equations 1.3 allows nonlinear internal resonances due to the interactions between the two oscillators, which may lead to a diverse range of behaviors in its four-dimensional phase space, including periodic, quasi-periodic, and chaotic responses (see, e.g., Thompson & Stewart, 1986).

The possibility for chaotic solutions to coupled oscillator models in general and equations 1.3 in particular has not been previously emphasized in the context of free rhythmic actions and suggests that it may be possible to account for experimentally observed temporal variability without relying on external noise inputs. Thus, this class of models can be used to address an open question regarding the origin of variability in free rhythmic actions and its relationship to observed steady-state dynamics (Riley & Turvey, 2002). Different viewpoints on this question center on different interpretations of the variability inherent in the rhythmic motions. A first viewpoint suggests that this variability is the result of stochastic influences in the neuromuscular system on otherwise periodic responses, whereas proponents of a second viewpoint suggest that the variability stems from an underlying chaotic dynamic.

The dichotomy between these viewpoints is reflected in the fundamentally different approaches taken in experimental studies. In order to test the hypothesis that chaotic dynamics underlies the observed ubiquitous fluctuations in biological data, nonlinear time-series analyses have been applied to experimental data. For example, dimensionality analyses of the

variability of free rhythmic actions in human hand-held pendulum swinging have pointed to positive maximum Lyapunov exponents and noninteger dimensions as evidence supporting this viewpoint (Mitra, Riley, & Turvey, 1997; Goodman, Riley, Mitra, & Turvey, 2000). However, these experimental methods are based on a priori assumptions that lead to questions about the interpretations of their results. In particular, all of these time-series analysis techniques were developed considering low-dimensional deterministic dynamics, and are thus difficult to usefully apply to high-dimensional, and possibly stochastic, experimental time series (Kantz & Schreiber, 2004). The opposing viewpoint that interprets the underlying dynamic of free rhythmic actions as periodic plus noise suffers from similar a priori assumptions. For example, studies that have used Floquet multipliers to analyze the stability properties of locomotion in humans (Hurmuzlu & Basdogan, 1994; Hurmuzlu, Basdogan, & Carollo, 1994) and greyhound dogs (Marghitu, Kincaid, & Rumph, 1996) have suggested the existence of stable fixed points in the Poincaré sections taken from the experimental time series, indicating a stable limit cycle in the original continuous time system. However, the assumption of the existence of an isolated periodic orbit underlying applications of Floquet theory is not justified if the underlying dynamic is chaotic or strongly stochastic. The nature of the problem is further illustrated by comparing the results of Hurmuzlu and colleagues to those of Dingwell and Cusumano (2000) who also analyzed the stability properties of human locomotion. Instead of Floquet multipliers, however, Dingwell and Cusumano made no a priori assumptions about the degree of determinism in the system and used maximum short-time Lyapunov exponents for their stability analyses, obtaining positive exponents for the data of walking individuals in their study. While the authors make it clear that their results do not necessarily indicate the presence of chaotic motions, neither is the result wholly compatible with the assumption that the underlying dynamic of human walking is primarily the result of a stable limit cycle.

In this letter, we present a new study of the coupled oscillator system of equations 1.3, which has previously been shown to account for the frequency scaling properties of free rhythmic actions, specifically human arm swinging movements (Hatsopoulos, 1996; Hatsopoulos & Warren, 1996). The analysis presented here covers the same region of parameter space as applied to account for the original empirical results, but is more systematic and includes a thorough examination of bifurcations between various types of dynamical behavior not previously noted in this model. The results of our analytical work contribute to the resolution of the apparent contradiction between the chaotic and "periodic plus noise" viewpoints on rhythmic movement. At the same time, the results show that frequency scaling is a much more robust phenomenon than previously noted and that it can effectively persist in a large region of the system's parameter space, even as the system undergoes bifurcations leading to chaotic steady

states. Based on our analysis, we are able to restate the question regarding the stochastic-deterministic nature of rhythmic actions as a question about where in parameter space such a model best represents experimental observations.

## 2 Methods

---

To facilitate analyses and gain further insight into the nature of the coupling of equations 1.3, the following dimensionless scaling was used:

$$\bar{t} = \lambda t \quad \bar{x} = \frac{\lambda^2}{G} x \quad \bar{y} = y, \quad (2.1)$$

in which it is assumed that the CPG variable  $y$  is already in dimensionless form. In addition, the following dimensionless parameter definitions were used:

$$a = \frac{\varepsilon}{\lambda} \quad b = \frac{\omega}{\lambda} \quad c = \frac{BG}{\lambda^3}, \quad (2.2)$$

yielding the rescaled system of equations with two parameters fewer than the original of equation 1.3:

$$\bar{y}'' + a(\bar{y}^2 - 1)\bar{y}' + (b + c\bar{x})^2\bar{y} = 0 \quad (2.3a)$$

$$\bar{x}'' + \bar{x} = \bar{y} \quad (2.3b)$$

Primes denote differentiation with respect to  $\bar{t}$ . In addition to the reduction in the number of parameters, a further benefit of using the rescaled system, equations 2.1 to 2.3, is that the biomechanical system's natural frequency has been normalized to unity, allowing a more direct examination of the robustness of the model's capacity for frequency scaling. Importantly, the rescaled system shows that it is only the ratio of the two oscillators' frequencies contained in the parameter  $b$  that is important, not the value of either frequency independently. Similarly, it is not the values of either of the coupling parameters  $B$  or  $G$  alone that will account for the qualitative properties of the solutions to equations 2.3, but rather their scaled product, as captured by the parameter definition of the coupling strength parameter  $c$ .

The values of the parameters (eq. 2.2) used in the derivation of the results reported in this study were  $a = 0.0995$ ,  $b \in [0.15, 0.24]$ ,  $c \in [0.13, 0.20]$ , which were chosen based on the previous simulations of Hatsopoulos (1996) as they satisfactorily modeled the observed empirical results. The system of differential equations 2.3 was numerically integrated using a fourth-order Runge-Kutta integrator with a variable time step. The solutions were

then sampled at a dimensionless frequency of 90. Absolute and relative error tolerances in the numerical computations were set to  $10^{-6}$ . All calculations and simulations were done in Matlab (MathWorks, Version 7). Since the experimental observable of the model 2.3 is the time evolution of the biomechanical oscillator, equation 2.3b, all of the following analyses are presented in terms of these state variables ( $\bar{x}(t)$ ,  $\bar{x}'(t)$ ). References to the state variables of the model in this letter will always refer to the rescaled system 2.3, although the overbars will be dropped for simplicity.

Bifurcation diagrams were created using coupling strength  $c$  as the control parameter for the range of values given above in increments of 0.0001, giving 700 values of  $c$  in total. For each value of  $c$ , the system, equations 2.3, was numerically integrated for approximately 600 natural periods ( $T = 2\pi$ ) of the biomechanical oscillator. The resulting first 300 cycles of the oscillator were discarded to ensure that transients had decayed. The values of the local maxima of the remaining approximately 300 cycles were plotted above each corresponding  $c$  value. Hence, a period- $N$  orbit of the biomechanical oscillator for a given value of  $c$  results in  $N$  distinct points in the bifurcation diagram plotted above that  $c$  value.

Qualitatively different solutions to equations 2.3 were plotted in the time domain, phase plane, and frequency domain using the position  $x(t)$  and velocity  $x'(t)$ . Before computing the power spectral density (PSD) of the steady-state response, a noise floor was added to the time series  $x(t)$  with a standard deviation of 1% of the original signal, allowing a better visual representation of the dominant components of the signals in the frequency domain. All frequency spectra are presented in terms of dimensionless angular frequencies. For a given solution, the local maxima of the time series  $x(t)$  were extracted to create approximate cycle amplitude probability densities, using 3000 local maxima for each histogram. For example, a period-1 orbit of the biomechanical oscillator results in a single bar in the amplitude histogram, since all local maxima have equal values.

Correlation dimensions and maximum Lyapunov exponents were estimated from representative solutions that appeared aperiodic in the bifurcation diagrams, indicating possible chaotic dynamics. All estimates were computed using the TISEAN software package (Hegger, Kantz, & Schreiber, 1999). Estimates for each chosen value of the control parameter  $c$  were obtained from 20 different solutions to equations 2.3 using randomly selected initial conditions. The results are reported as the means plus or minus standard errors of the 20 estimates. To check for accuracy of the results in the dimension and exponent calculations, a control parameter value that resulted in period-1 solutions was included.

Spectral bifurcation diagrams were created along with the bifurcation diagrams, using  $c$  as the control parameter. The spectral bifurcation diagram displays the PSD of the biomechanical oscillator's steady-state response as a function of frequency and the control parameter  $c$ . As these are three-dimensional plots, false color was used to display the results, with the

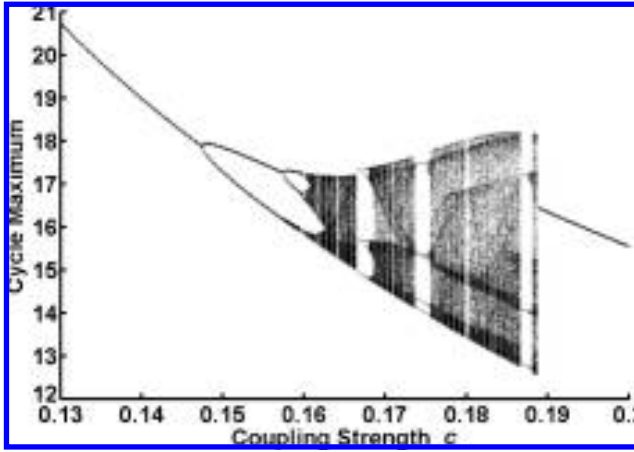


Figure 1: Bifurcation diagram for equations 2.3 with van der Pol frequency  $b = 0.2$ . Local maxima for approximately 300 cycles of the biomechanical oscillator are plotted over each value of the parameter  $c$  in increments of 0.0001.

color map indicating the spectral amplitude. Computing the spectral bifurcation diagram allows one to examine the frequency scaling behavior of equations 2.3 as the control parameter  $c$  is changed. Frequency scaling is indicated when the fundamental frequency of the biomechanical oscillator's response is located at a constant dimensionless angular frequency (represented by a vertical line in the spectral bifurcation diagram) for a range of  $c$  values, indicating that the ratio between the CPG and pendulum frequencies is constant. For example, scaling at exactly the natural frequency occurs when the fundamental response frequency has a constant value of 1, since the natural frequency of the biomechanical oscillator has been normalized to unity in equations 2.3.

### 3 Results

---

Figure 1 displays the bifurcation diagram for the uncoupled van der Pol frequency parameter  $b = 0.2$ . A period-doubling sequence of bifurcations can be seen for increasing values of coupling strength  $c$ . This cascade of period doublings can be further observed in the time series, phase planes, frequency spectra, and cycle amplitude histograms of the biomechanical oscillator. Figures 2, 3, and 4 show representative cases for the period-1 ( $c = 0.14$ ), period-2 ( $c = 0.154$ ), and period-4 ( $c = 0.159$ ) orbits, respectively. Note that the uniqueness of solutions is not violated by the intersections visible in the plots since these are projections of the four-dimensional phase space of the system 2.3 into the plane.

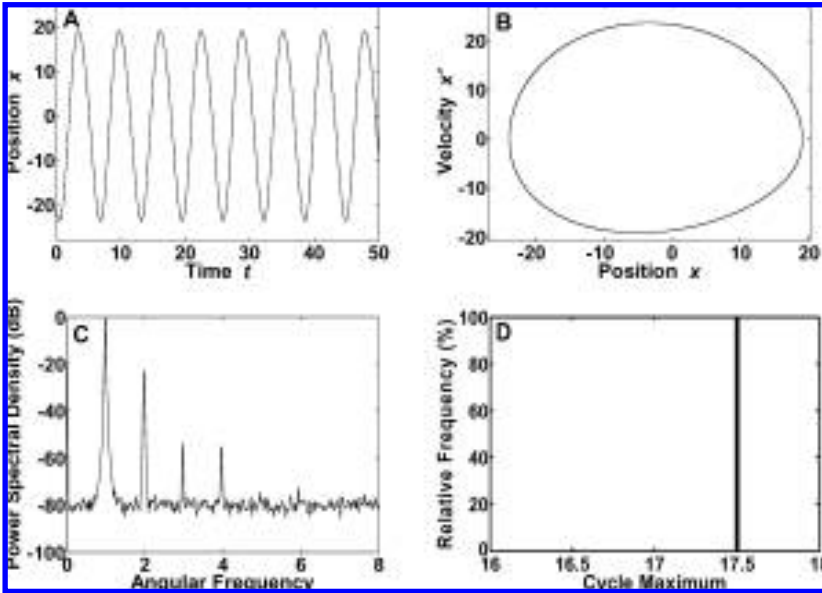


Figure 2: (A) Time series. (B) Phase plane. (C) Power spectrum. (D) Cycle maximum histogram for a period-1 solution with parameters  $b = 0.2, c = 0.14$ .

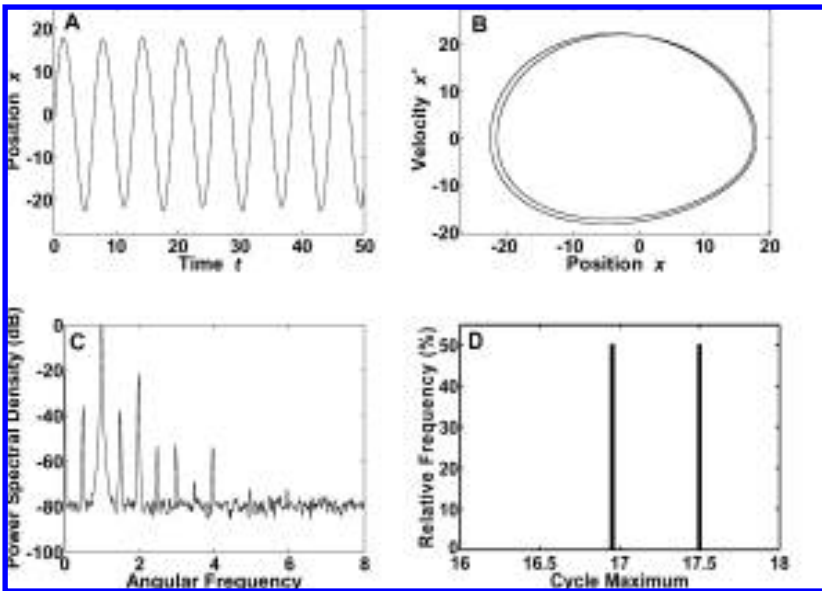


Figure 3: (A) Time series. (B) Phase plane. (C) Power spectrum. (D) Cycle maximum histogram for a period-2 solution with parameters  $b = 0.2, c = 0.154$ .

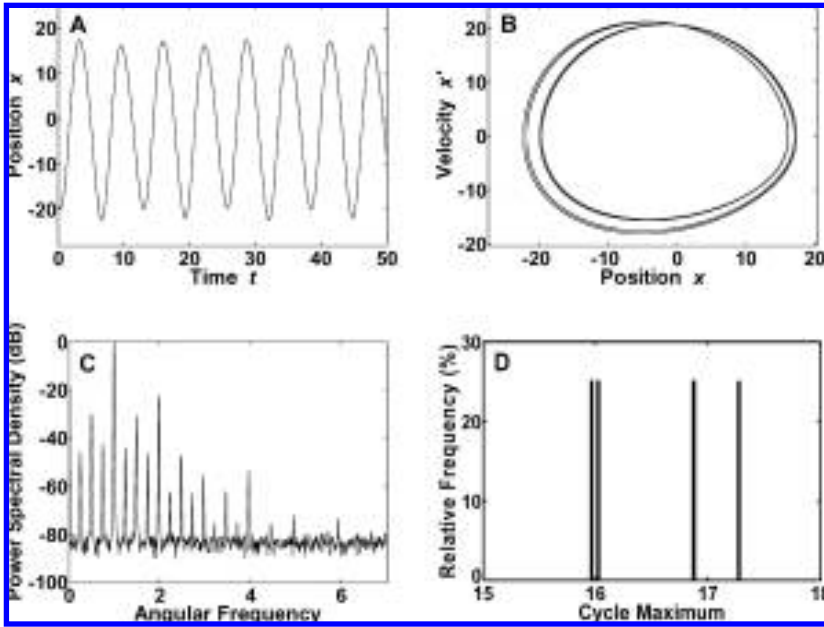


Figure 4: (A) Time series. (B) Phase plane. (C) Power spectrum. (D) Cycle maximum histogram for a period-4 solution with parameters  $b = 0.2$ ,  $c = 0.159$ .

The figures offer different ways of viewing the period-doubling structure. For example, the time series in Figures 2A, 3A, and 4A show that the period doublings can be seen as slight, periodic modulations of the cycle amplitudes. The phase planes in Figures 2B, 3B, and 4B show this same result indicated by the number of orbits in the plane before the trajectory closes on itself. In the power spectra of Figures 2C, 3C, and 4C, bifurcations are indicated by the appearance of subharmonics. Finally, Figures 2D, 3D, and 4D show the period doublings as the appearance of additional bars in the histograms.

The bifurcation diagram in Figure 1 also shows periodic windows interspersed between the intervals with aperiodic long-term behavior of the biomechanical oscillator. For example at  $c = 0.1667$  a period-3 cycle can be observed, which is then followed by another period-doubling cascade as  $c$  is increased. Figure 5 shows a magnification of this sequence of period doublings for the middle branch of the period 3 cycle for  $c \in [0.1665, 0.1685]$ . The fine-scale structure apparent in Figure 5 that is similar to the larger scale in Figure 1 illustrates fractal properties of the solutions to equations 2.3.

The period-doubling sequence suggests that the system 2.3 may be governed by chaotic dynamics in the intervals of the bifurcation diagram that show aperiodic trajectories of the biomechanical oscillator. To confirm this,

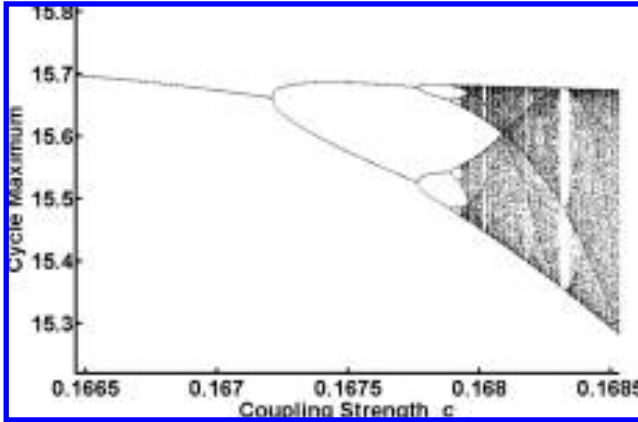


Figure 5: Magnification of the middle branch of the period-3 window in Figure 1.

Table 1: Correlation Dimension and Maximum Lyapunov Exponent Estimates for a Representative Period 1 ( $c = 0.14$ ) and Two Aperiodic ( $c = 0.163, 0.178$ ) Solutions to Equations 2.3, with Parameter  $b = 0.2$  for All Three Solutions.

Coupling Strength ( $c$ )	Correlation Dimension	Maximum Lyapunov Exponent
0.140	1.0011 (0.0013)	0.0000 (0.0000)
0.163	2.0105 (0.0058)	0.0533 (0.0016)
0.178	2.0224 (0.0064)	0.0602 (0.0031)

Note: Results are reported as mean  $\pm$  standard error.

correlation dimensions and maximum Lyapunov exponents were determined from the solutions for two different values of the parameter  $c$  within the aperiodic intervals. The results are reported in Table 1 by the means  $\pm$  standard errors of the estimates to the given number of significant digits. The estimates for the period-1 solutions are consistent with limit cycle dynamics (i.e., dimension equal to 1; maximum Lyapunov exponent equal to 0) and indicate the reliability and accuracy of the algorithms. The noninteger correlation dimensions greater than two and the positive Lyapunov exponents for the aperiodic solutions confirm that the trajectories are chaotic. The correlation dimensions just slightly greater than two for the chaotic solutions are consistent with the high amount of dissipation in the system due to the van der Pol’s nonlinear damping term. The reduction of dimensionality due to phase-space volume contraction is a well-known characteristic of multidimensional systems that display period-doubling routes to chaos (Cvitanovic, 1989).

This effect can also be seen in the return maps in Figures 6A and 6B, which were created by plotting successive local maxima of the chaotic

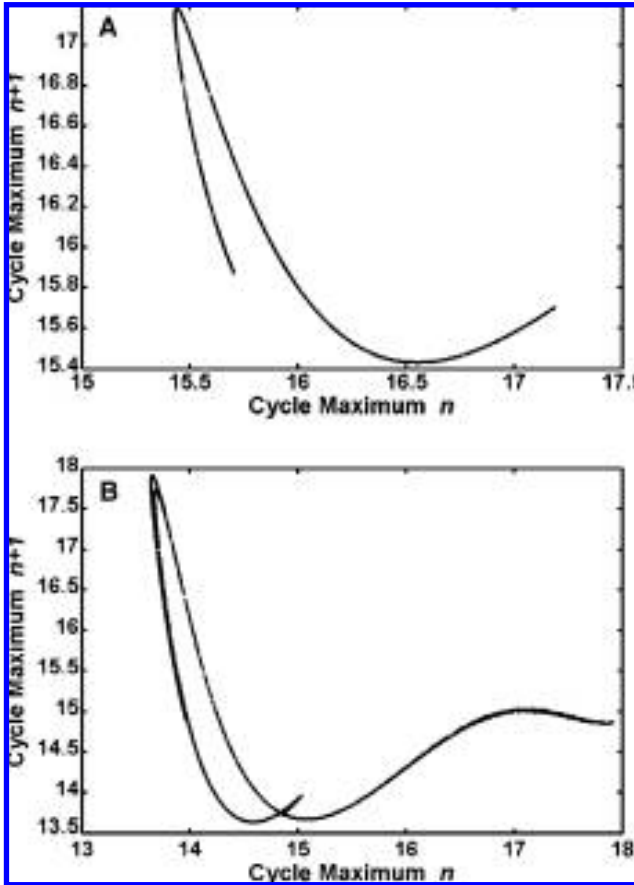


Figure 6: Return maps created from chaotic solutions to equation 2.2 using consecutive local maxima of the biomechanical oscillator with parameters. (A)  $b = 0.2, c = 0.163$ . (B)  $b = 0.2, c = 0.178$ .

trajectories against each other. The figures show locally a nearly one-dimensional relationship between successive local maxima of the chaotic solutions, again indicating the collapse of dimensionality due to dissipation. Time series, phase planes, power spectra, and amplitude histograms are shown in Figures 7 and 8 for the two representative chaotic solutions.

Of particular relevance to this study is the fact that the time series in Figures 7A and 7B show that the chaos is represented by only small, irregular fluctuations in amplitude from cycle to cycle. The phase-plane plots in Figures 7B and 8B indicate this by the apparent bands filled out by the trajectories. The power spectra in Figures 7C and 8C show continuous spectral

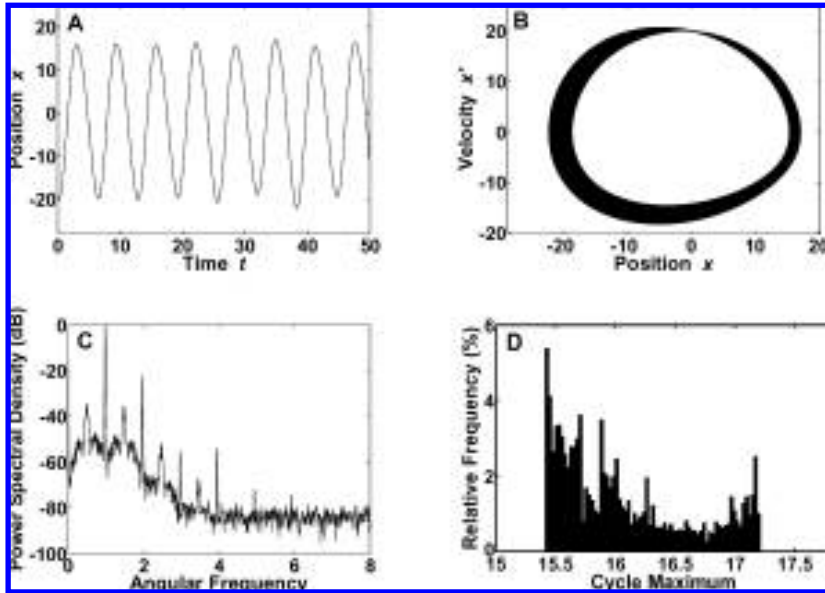


Figure 7: (A) Time series. (B) Phase plane. (C) Power spectrum. (D) Cycle maximum histogram for a chaotic solution with parameters  $b = 0.2, c = 0.163$ .

amplitudes above the noise floor for a range of angular frequencies below 3. The amplitude histograms in Figures 7D and 8D show a continuous, nonnormal distribution of cycle amplitudes.

The significance of this weakly chaotic dynamics, wherein an otherwise periodic response has a small amount of chaotic amplitude modulation, is further illustrated by the spectral bifurcation diagram of Figure 9A, which corresponds to the bifurcation diagram of Figure 1 created using local maxima. However, in the spectral bifurcation diagram, the horizontal line at each fixed value of the bifurcation parameter  $c$  is a false color representation of the PSD for the corresponding steady-state solution. The figure shows that the periodic orbits for all values of  $c$  up to 0.1473 have a fundamental angular frequency equal to 1 and, hence, are locked at the biomechanical oscillator’s natural frequency. After the initial period-doubling bifurcation, the appearance of subharmonics in the power spectra destroys this “strict” frequency scaling. However, the false color plot indicates that almost all spectral power remains at the natural frequency throughout the bifurcations away from periodic solutions: the next highest peak in the PSD in these regions is over 30 dB lower than the frequency 1 peak (i.e., in amplitude, it is smaller by a factor of more than 30). That is, although the chaotic solutions are aperiodic with continuous power spectra throughout a range of frequencies, the spectral peaks at the biomechanical oscillator’s natural

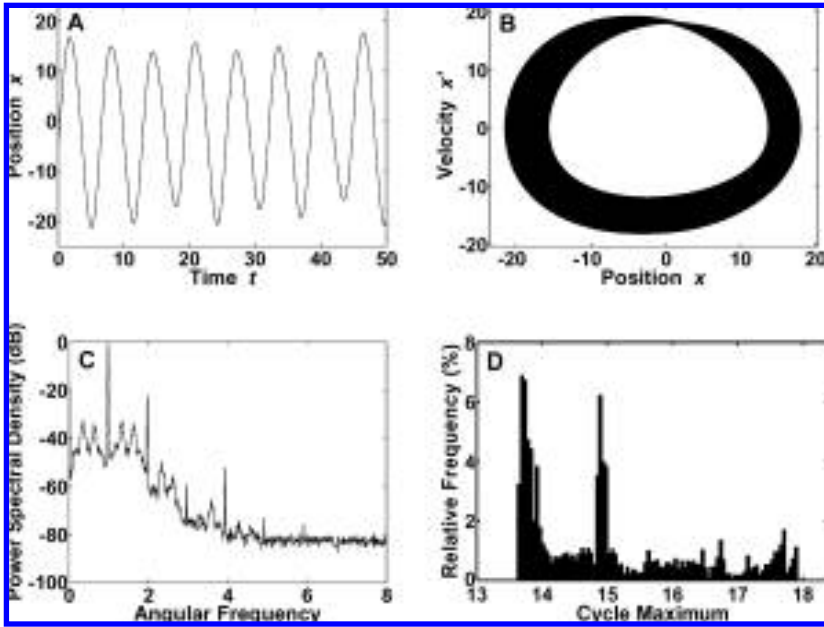


Figure 8: (A) Time series. (B) Phase plane. (C) Power spectrum. (D) Cycle maximum histogram for a chaotic solution with parameters  $b = 0.2$ ,  $c = 0.178$ .

frequency are over 30 dB higher than those at all other frequencies. Hence, the *effective* (i.e., dominant) frequency of the responses is seen to scale with the natural frequency throughout the entire bifurcation sequence.

To test the robustness of the results, bifurcation diagrams and spectral bifurcation diagrams were created for different values of the uncoupled van der Pol frequency  $b$ , again with coupling strength  $c$  as the control parameter. The results were qualitatively similar to those displayed in Figures 1 and 9, although the locations of the bifurcation points were different. Figure 10 shows the bifurcation points in the  $b$ - $c$  parameter plane for the first two period doublings for all values of the parameter  $b$  used in this analysis. Also included in the figure are the points where maximum Lyapunov exponents first became positive, using a threshold of 0.0001. (Note that the bifurcation and positive maximum Lyapunov exponent points were calculated only for the points indicated by markers, and the lines connecting the points are simply meant to serve as visual aids.) Figure 10 indicates that the range of qualitative behaviors illustrated in Figures 1 to 9, and their overall organization, persists throughout the entire region of parameter space. In particular, the scaling of the dominant response frequency to the biomechanical natural frequency is seen to be far more robust than previously imagined.

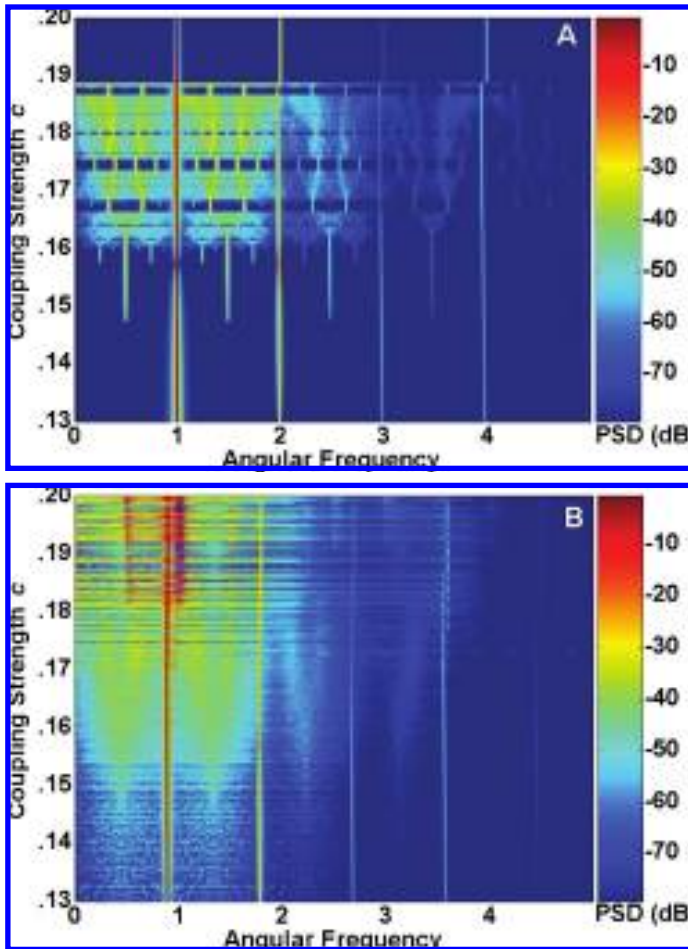


Figure 9: Spectral bifurcation diagrams displaying the power spectral density (PSD) of the biomechanical oscillator's steady-state response as a function of the control parameter,  $c$ , and dimensionless angular frequency. (A) Results corresponding to the solutions represented in Figure 1. (B) Results for the same system parameters as Figure 1, but with added process noise (see also Figure 11).

#### 4 Discussion

---

This study has examined the dynamics of a coupled oscillator model originally proposed by Hatsopoulos (1996) for free rhythmic action in human arm swinging. This model was previously shown to successfully capture a key feature of free rhythmic arm swinging in humans, namely, resonance

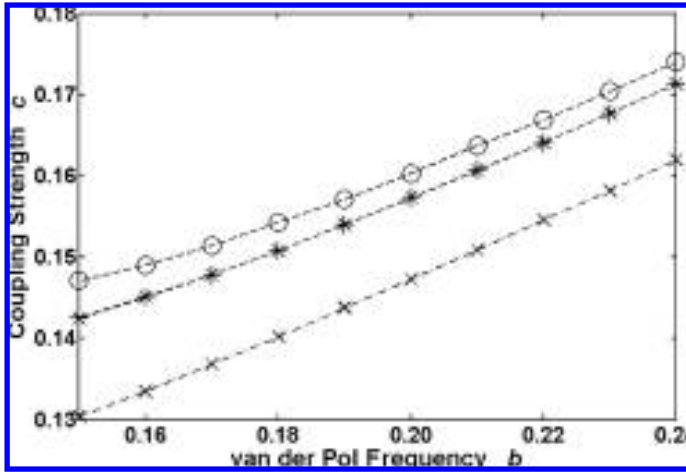


Figure 10: Bifurcation points in the  $b$ - $c$  parameter plane for the first ( $\times$ ) and second ( $*$ ) period-doubling bifurcations, as well as the points where maximum Lyapunov exponents first become positive ( $o$ ).

tuning or frequency scaling—the preference to select an oscillation frequency corresponding to the natural frequency of the limb (Hatsopoulos & Warren, 1996). The comprehensive numerical reexamination of the model carried out in this letter has revealed the full range of behaviors possible in such a system, including period-doubling bifurcation sequences leading to chaotic oscillations. More important and beyond the observation of these previously unnoted behaviors, however, our discovery of weakly chaotic dynamics in the Hatsopoulos oscillator suggests the resolution of an outstanding paradox in the modeling of free rhythmic actions: How can one model experimentally observed frequency scaling, which seems to require periodic oscillations, and simultaneously account for the temporal variability observed in experiments without the addition of ad hoc noise sources? Our results demonstrate that coupled oscillator models can produce robust oscillations with a small chaotic modulation that provide both effective frequency scaling and a deterministic source of temporal variability.

Further, the rescaling of the system via equations 2.2 not only made the exploration of the system's parameter space more efficient, but also indicated that it is the ratios of certain parameters, and not their absolute values, that are important for determining the properties of the solutions. In particular, normalizing the natural frequency of the biomechanical oscillator to unity revealed the robustness of frequency scaling by means of the spectral bifurcation diagrams of Figure 9. The spectral bifurcation diagram of Figure 9A showed that, as expected, the fundamental frequencies of the period-1 solutions to equation 2.3 are equal to the biomechanical oscillator's

natural frequency, which we term *strict frequency scaling*. However, the diagram also shows that throughout the entire parameter range studied and across all bifurcations, including into regions of aperiodic dynamics, the amplitude at the natural frequency remains over 30 times higher than those at all other frequencies. This significant difference in amplitudes shows that although strict frequency scaling no longer holds, *effective frequency scaling* is maintained at the biomechanical level.

Based on these results, we suggest that effective frequency scaling is the only form that has been measured in experiments. Conventional methods of experimentally determining oscillation frequencies, using averages of peak-to-peak periods or the global peak in the power spectral density, would consider the period-1, subharmonic, and chaotic solutions to equations 2.3 as equal evidence, within experimental error, for frequency scaling. Thus, our more general notion of effective frequency scaling, which is more consistent with experimental practice than definitions derived from purely analytical considerations, shows the Hatsopoulos model to be capable of frequency scaling while concurrently displaying temporal variability in the biomechanical oscillator's waveforms. This finding may open the possibility of reconciling the findings in the literature on a stable neuromechanically determined preferred frequency with studies that have focused on the existence or nonexistence of chaotic structure underlying the spatiotemporal variability of free rhythmic actions (Riley & Turvey, 2002).

Based on our results, the question can be whether free rhythmic actions are best modeled by areas of parameter space that show limit cycle dynamics or rather by areas that show chaotic dynamics. If the variability of free rhythmic action has an underlying chaotic dynamic that is consistent with the model proposed by Hatsopoulos (1996), then our results suggest that this underlying dynamical structure can be captured in return maps and histograms constructed from the peak-to-peak amplitudes of the positional time series.

However, it is possible that any low-dimensional chaotic structure in return maps created from experimental time series may be lost due to measurement or dynamical noise processes, or both. Indeed, the physiological systems that produce these behaviors are complex and high-dimensional, and the behavior may have to be treated as operationally stochastic despite underlying deterministic structure. Note that while it has been emphasized that autonomous equations of motion are needed to gain fundamental insight into how free rhythmic actions are produced, this does not imply that there is no role for stochastic influences in the current models.

To explore the experimental implications of our theoretical results in the presence of noise, we added a stochastic forcing term to the van der Pol oscillator in equations 2.3 to represent high-dimensional inputs to the CPG. This stochastic term consisted of a gaussian random variable with zero mean and a standard deviation of 1.3 (about 40% of the typical van der Pol output). The random variable was approximated in the simulations by a

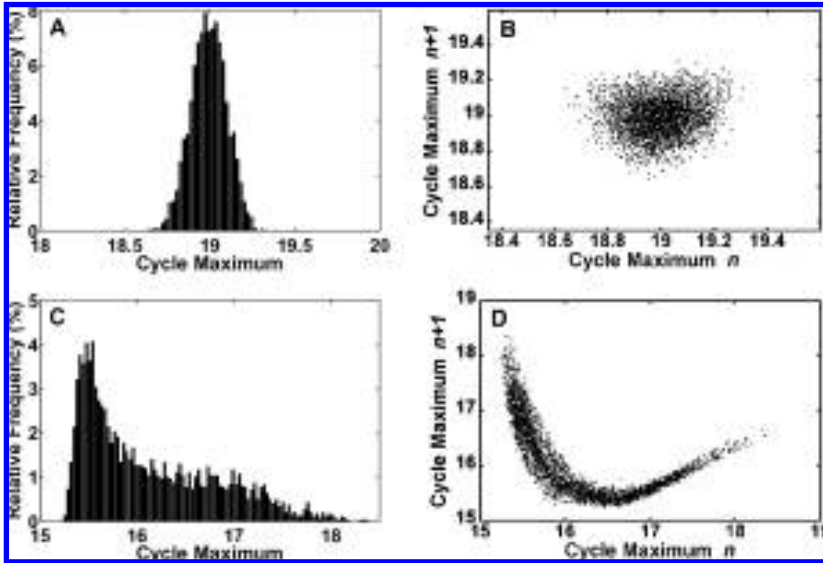


Figure 11: (A) Cycle maximum histogram. (B) Return map for a period 1 solution ( $b = 0.2$ ,  $c = 0.14$ ) with added process noise. (C) Cycle maximum histogram. (D) Return map for a chaotic solution ( $b = 0.2$ ,  $c = 0.163$ ) with added process noise.

quasiperiodic series with 100 terms and angular frequencies ranging from 0 to  $20\pi$ , using the Kac-Shinozuka representation (Simiu, 2002). We then recomputed the amplitude histograms and the return maps.

Figure 11 shows the results for the system of equations 2.3 with the added stochastic term, computed for parameter values corresponding to period-1 (see Figures 11A and 11B) and chaotic solutions when the stochastic perturbation is not present (see Figures 11C and 11D). It can be seen that in this case, if free rhythmic actions were governed by limit cycle dynamics with added gaussian noise, then the amplitude histogram should show an approximately normal distribution. Correspondingly, the return map should show an approximately elliptical cloud of points. If, however, free rhythmic actions have an underlying chaotic dynamic, then the amplitude histogram can be expected to have a strongly skewed, nonnormal distribution. In addition, the variability in the data in the return map should be distributed along the underlying attractor and hence not localized around a single spot. In our results, this chaotic attractor is represented by a crescent shape.

Finally, we again computed the entire spectral bifurcation diagram with parameters identical to those used for Figures 1 and 9A, but with noise input as described above. The result is shown in Figure 9B. It is seen that the key qualitative features of the noise-free diagram were preserved: for

all values of  $c$  used, the power spectra were dominated by a single peak and its harmonics, and effective frequency scaling was maintained. To be sure, small quantitative differences can be discerned with the added noise: the peak of the fundamental frequency is shifted down about 10%, to a value of around 0.9, and the higher noise floor results in this peak being only about 15 times higher than the spectral components at frequencies away from it or its harmonics, compared to a factor of over 30 without input noise as in Figure 9A. Nevertheless, despite these small differences, the overall robustness of effective frequency scaling is clearly demonstrated in the presence of input noise for the range of parameter values associated with both periodic and chaotic responses in the noise-free case.

While we do not expect these results to exactly match human subject data, they suggest that important qualitative information about the nature of variability in free actions can be obtained in experiments by inspecting the data as exemplified in Figure 11, using return maps and probability density functions. While in principle these analyses pose no difficulty, they may suffer from the typical problems of more sophisticated variability analysis, that is, measurement noise and the need for sufficiently large amounts of data. Yet it may be possible to overcome these inherent difficulties with well-designed conditions corresponding to distinct dynamical states that bring out the differences in distributions similar to Figures 11.

To gain further insight, it may help to speculate why evolutionary constraints should favor one particular dynamic over the other to govern free rhythmic actions. Researchers that view free rhythmic actions as periodic processes emphasize the robustness and stability of limit cycle dynamics (Hurmuzlu et al., 1994; Kay et al., 1987; Marghitsu et al., 1996), consistent with the theoretical viewpoint in the field of motor control that dynamic stability plays an important role in the coordination of movement behaviors (e.g., Holt, Jeng, Ratcliffe, & Hamill, 1995; Patla & Sparrow, 2000; Sternad, Duarte, Katsumata, & Schaal, 2000). Researchers who view the rhythmic motions as chaotic also emphasize the role of stability, but they place additional emphasis on the inherent adaptability and flexibility of movement systems in the changing environment. For instance, Rabinovich and Arbarbanel (1998) suggest that the local instabilities of chaotic dynamics may offer a biological system the needed flexibility by allowing the exploration of a greater area of its phase space than is possible with limit cycle dynamics (see also Beek, 1996). This may allow transitions between different patterns of behavior when the environment requires it. Proponents of the limit cycle dynamics with noise perspective, however, may counter this argument by pointing out that stochastic fluctuations in deterministic systems may similarly facilitate transitions between behaviors. This point has been illustrated in the context of the Haken-Kelso-Bunz model for bimanual rhythmic coordination where the addition of the stochastic term was needed to simulate transitions from antiphase to in-phase behavior (Schöner, Haken, & Kelso, 1986; Haken, Kelso, & Bunz, 1985).

This line of reasoning suggests that both viewpoints offer sound arguments concerning the nature of the variability observed in free rhythmic actions. Which one is ultimately the appropriate paradigm for understanding the variability must be determined on the basis of empirical results. Analysis of the structure of variability in experimental time series should provide more insight. However, time-series analysis techniques require a number of assumptions that are hard to satisfy in experimental time series. Yet they are easily satisfied in their corresponding mathematical models. Hence, this theoretical study of a coupled oscillator model demonstrates one alternative strategy of examining the presence or absence of chaos. By example, we showed that the variability observed in experimental data on free rhythmic actions may in principle be considered of chaotic origin.

### Acknowledgments

---

The work of A. R. and D. S. was made possible by grants from the National Science Foundation (BCS-0450218), the National Institutes of Health (RO1-HD045639), and the Office of Naval Research (N00014-05-1-0844). J. C.'s work was partially supported by National Science Foundation grant CMS-0625764.

### References

---

- Beek, P. J. (1996). Dexterity in cascade juggling. In M. L. Latash & M. T. Turvey (Eds.), *Dexterity and its development* (pp. 377–392). Mahwah, NJ: Erlbaum.
- Beek, P. J., & Beek, W. (1988). Tools for constructing dynamic models of rhythmic movement. *Human Movement Science, 7*, 301–342.
- Beek, P. J., Peper, C. E., & Daffertshofer, A. (2002). Modeling rhythmic interlimb coordination: Beyond the Haken-Kelso-Bunz model. *Brain and Cognition, 81*(1), 149–165.
- Cvitanovic, P. (1989). Universality in chaos. In P. Cvitanovic (Ed.), *Universality in chaos* (2nd ed.). Bristol and Philadelphia: Institute of Physics Publishing.
- Demont, M. E. (1988). Tuned oscillations in the swimming scallop *Pecten maximus*. *Canadian Journal of Zoology, 68*, 786–791.
- Demont, M. E., & Gosline, J. M. (1988). Mechanics of jet propulsion in the hydromedusa jellyfish, *Polyorchis penicillatus*. *Journal of Experimental Biology, 134*, 347–361.
- Dennett, D. C. (1971). Intentional systems. *Journal of Philosophy, 68*, 87–106.
- Dingwell, J. B., & Cusumano, J. P. (2000). Nonlinear time series analysis of normal and pathological human walking. *Chaos, 10*, 848–863.
- Goldfield, E. C., Kay, B. A., & Warren, W. H., Jr. (1993). Infant bouncing: The assembly and tuning of action systems. *Child Development, 64*, 1128–1142.
- Goodman, L., Riley, M., Mitra, S., & Turvey, M. T. (2000). Advantages of rhythmic movements at resonance: Minimal active degrees of freedom, minimal noise, and maximal predictability. *Journal of Motor Behavior, 32*, 3–8.
- Greenewalt, C. H. (1960). The wings of insects and birds as mechanical oscillators. *Proceedings of the American Philosophical Society, 104*, 605–611.

- Haken, H., Kelso, J. A. S., & Bunz, H. (1985). A theoretical model of phase transitions in human hand movements. *Biological Cybernetics*, *51*, 347–356.
- Hatsopoulos, N. G. (1996). Coupling the neural and physical dynamics in rhythmic movements. *Neural Computation*, *8*, 567–581.
- Hatsopoulos, N. G., & Warren, W. H. (1996). Resonance tuning in rhythmic arm movements. *Journal of Motor Behavior*, *28*, 1, 3–14.
- Hegger, R., Kantz, H., & Schreiber, T. (1999). Practical implementation of nonlinear time series analysis methods: The TISEAN package. *Chaos*, *9*(2), 413–435.
- Holt, K. G., Hamill, J., & Andres, R. O. (1990). The force-driven harmonic oscillator as a model for human locomotion. *Human Movement Science*, *9*, 55–68.
- Holt, K. G., Jeng, S. F., Ratcliffe, S. F., & Hamill, J. (1995). Energy cost and stability during human walking at the preferred stride frequency. *Journal of Motor Behavior*, *26*, 164–178.
- Holt, K. G., Saltzman, E., Ho, C. L., Kubo, M., & Ulrich, B. D. (2006). Discovery of the pendulum and spring dynamics in the early stages of walking. *Journal of Motor Behavior*, *38*(3), 206–218.
- Hurmuzlu, Y., & Basdogan, C. (1994). On the measurement of dynamic stability of human locomotion. *Journal of Biomedical Engineering*, *116*, 30–36.
- Hurmuzlu, Y., Basdogan, C., & Carollo, J. (1994). Presenting joint kinematics of human locomotion using phase plane portraits and the Poincaré maps. *Journal of Biomechanics*, *27*, 1495–1499.
- Kantz, H., & Schreiber, S. (2004). *Nonlinear time series analysis*. Cambridge: Cambridge University Press.
- Kay, B. A., Kelso, J. A. S., Saltzman, E. L., & Schönner, G. (1987). Space-time behavior of single and bimanual rhythmical movements: Data and limit cycle model. *Journal of Experimental Psychology: Human Perception and Performance*, *13*, 178–192.
- Kugler, P. N., & Turvey, M. T. (1987). *Information, natural law, and the self-assembly of rhythmic movements*. Hillsdale, NJ: Erlbaum.
- Marghitu, D. B., Kincaid, S. A., & Rumph, P. F. (1996). Nonlinear dynamics stability measurements of locomotion in healthy greyhounds. *American Journal of Veterinary Research*, *57*, 1529–1535.
- Mitra, S., Riley, M., & Turvey, M. T. (1997). Chaos in human rhythmic movement. *Journal of Motor Behavior*, *29*, 195–198.
- Patla, A. E., & Sparrow, W. A. (2000). Factors that have shaped human locomotor structure and behavior: The “joules” in the crown. In W. A. Sparrow (Ed.), *Energetics of human activity*. Champaign, IL: Human Kinetics.
- Rabinovich, M. I., & Arbarbanel, H. D. I. (1998). The role of chaos in neural systems. *Neuroscience*, *87*, 5–14.
- Riley, M., & Turvey, M. T. (2002). Variability and determinism in motor behavior. *Journal of Motor Behavior*, *34*, 99–125.
- Schöner, G., Haken, H., & Kelso, J. A. S. (1986). A stochastic theory of phase transitions in human hand movement. *Biological Cybernetics*, *64*, 442–452.
- Scripture, E. W. (1899). Observations on rhythmic action. *Science*, *10*(257), 807–811.
- Simiu, E. (2002). *Chaotic transitions in deterministic and stochastic dynamical systems*. Princeton, NJ: Princeton University Press.
- Sternad, D., Duarte, M., Katsumata, K., & Schaal, S. (2000). Dynamics of a bouncing ball in human performance. *Physical Review E*, *63*, 011902.

- Sternad, D., Saltzman, E. L., & Turvey, M. T. (1998). Interlimb coupling in a simple serial behavior: A task dynamic approach. *Human Movement Science, 17*, 393–433.
- Thompson, J. M. T., & Stewart, H. B. (1986). *Nonlinear dynamics and chaos: Geometrical methods for engineers and scientists*. Chichester: Wiley.
- Wenderoth, N., & Bock, O. (1999). Load dependence of simulated central tremor. *Biological Cybernetics, 80*, 285–290.
- Williamson, M. M. (1998). Neural control of rhythmic arm movements. *Neural Networks, 11*, 1379–1394.
- Yu, H., Russell, D. M., & Sternad, D. (2003). Task-effector asymmetries in a rhythmic continuation task. *Journal of Experimental Psychology: Human Perception and Performance, 29*(3), 616–630.

---

Received August 23, 2006; accepted February 5, 2007.

**This article has been cited by:**